Plasmon-enhanced UV photocatalysis

Mitsuhiro Honda,[1] Yasuaki Kumamoto,[2] Atsushi Taguchi,[2,3] Yuika Saito,[1,a)] and Satoshi Kawata[1]
[1]*Department of Applied Physics, Osaka University, Suita, Osaka 565-0871, Japan*
[2]*Nanophotonics Laboratory, RIKEN, Wako, Saitama 351-0198, Japan*
[3]*Department of Mechanical Systems Engineering, School of Engineering, Tokyo University of Agriculture and Technology, Koganei, Tokyo 184-8588, Japan*

(Received 17 October 2013; accepted 24 January 2014; published online 11 February 2014)

We report plasmonic nanoparticle enhanced photocatalysis on titanium dioxide (TiO_2) in the deep-UV range. Aluminum (Al) nanoparticles fabricated on TiO_2 film increases the reaction rate of photocatalysis by factors as high as 14 under UV irradiation in the range of 260–340 nm. The reaction efficiency has been determined by measuring the decolorization rate of methylene blue applied on the TiO_2 substrate. The enhancement of photocatalysis shows particle size and excitation wavelength dependence, which can be explained by the surface plasmon resonance of Al nanoparticles. © *2014 AIP Publishing LLC*. [http://dx.doi.org/10.1063/1.4864395]

Photocatalysis is an efficient method to chemically harness the energy from the sun.[1] A photocatalyst traps the photons to generate electron-hole pairs and subsequently induce chemical reactions at the surface. A promising photocatalyst that has been receiving considerable attention is titanium dioxide (TiO_2) because of its strong oxidizing power as well as physical and chemical stability.[2] TiO_2 has been used in a variety of environmental applications such as self-cleaning surfaces, water splitting, disinfection, and air purification.[3–6] Despite these several demonstrations, the photocatalytic activity of TiO_2 needs to be improved in order to make it a practical solution for many green- and energy-related problems.

One approach to increase the photocatalytic activity of TiO_2 is through plasmonics. In plasmonics, the excitation of localized surface plasmons (LSP) on the surface of metallic nanostructures produces intense electric field amplitudes that can increase light absorption,[7] thereby, improving the photocatalytic activities of TiO_2. Typical materials utilized for plasmonics are noble metals (Au, Ag, and Cu) which exhibit high enhancements in the visible light region. Although plasmonic photocatalysis has been demonstrated using Ag,[8,9] the improvement effects were not sufficiently high because the plasmon resonance wavelength is out of the absorption band of TiO_2 (3.2 eV). Since light absorption of TiO_2 is high in the deep-UV range, it is expected that the photocatalytic performance of TiO_2 would be enhanced more if the plasmonic metal used has resonance wavelength in the UV range as well. Recently, there have been efforts to expand plasmonics to the UV region.[10–14] Poor metals such as Al, In, Ga, Sn, Tl, Pb, and Bi have been found to exhibit plasmonic properties in the UV range.[15] Among these metals, Al is the best choice in terms of practical use because of its low toxicity and high stability in air.[10]

In this Letter, we report plasmonic photocatalysis of TiO_2 in the UV range by using UV-resonant aluminum nanoparticles (NPs). The reaction rate of photocatalysis increased by a factor as high as 14, and the photocatalytic enhancement depended on the particle size and irradiation wavelength. To examine further the relationship between the size of the nanoparticle and surface plasmon resonance, discrete dipole approximation (DDA) simulations were performed.

Figure 1 illustrates the concept of plasmon-enhanced photocatalysis. Briefly, a thin film of TiO_2 was deposited on a quartz substrate. Hexagonal patterns of Al nanoparticles were then formed on the surface of the TiO_2 film as shown in the inset using a lithographic method. To evaluate the photocatalytic activity, a test sample of methylene blue (MB) was applied to the substrate. By irradiating UV light from above the substrate, an enhanced field is generated in the vicinity of the Al nanoparticles, exciting the TiO_2 with an accelerated reaction rate.

The TiO_2 thin film was prepared by spin-coating anatase TiO_2 nanocrystals (Titania Coating, Tayca Corporation, suspended in water) with a diameter of 6 nm on a quartz substrate. The spin-coating speed and time were 7000 rpm and 30 s, respectively. This process formed a TiO_2 film with a thickness of ~150 nm.

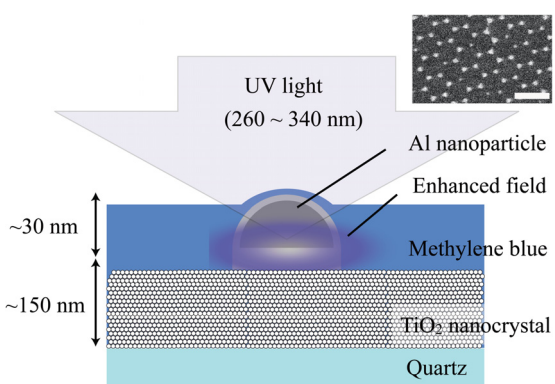

FIG. 1. Schematic view of plasmon-enhanced photocatalyst. Al nanoparticles are placed on TiO_2 film that consists of ~6 nm nanocrystals. UV lamp illuminates the sample from the side of methylene blue layer. The enhanced field is generated in the vicinity of the Al nanoparticles. The shape of Al nanoparticles is approximated as either hemispherical or triangular. The inset shows a SEM image of hexagonally aligned Al nanoparticles. The scale bar indicates 500 nm.

a)Author to whom correspondence should be addressed. Electronic mail: yuika@ap.eng.osaka-u.ac.jp.

For precise control of the size of metallic nanostructures, we employed the nanosphere lithography (NSL) technique.[16,17] Polystyrene (PS) beads were aligned into a hexagonal close-packing arrangement on the TiO_2 film by spin-coating. PS beads with diameters of 107 ± 2 nm, 147 ± 7 nm, and 336 ± 8 nm (Microparticles GmbH) were used to investigate the size effect of the Al nanoparticles on plasmon resonance. After that, Al was deposited on the substrate by thermal evaporation of an Al wire (99.99% purity) in vacuum conditions ($\sim 2 \times 10^{-4}$ Pa). The evaporation speed was adjusted to 0.1 Å/s monitored with a quartz crystal microbalance. The deposition thickness was 30 nm. The PS beads were then removed by sonication in toluene for 1 min. With the 107 nm and 147 nm diameter PS beads, the shapes of the structures were hemispherical, and with the 336 nm diameter PS beads, the shape of the structure was triangular. The maximum widths were 28, 34, and 80 nm in ascending order of the PS bead size. Finally, to monitor the speed of the reactions, MB aqueous solution (200 mM) was spin-coated on the substrate at 7000 rpm for 30 s.

The photocatalytic reaction was initiated by irradiating the structures with UV light. The UV light source was a laser-driven light source (LDLS EQ-99, Tokyo Instruments, Inc.), which has a broad uniform spectrum from 170 nm to 800 nm. To avoid the effects of visible light, e.g., heat, UV light ranging from 260 to 340 nm was extracted with a bandpass filter. The total intensity of the UV light was 8.1 mW/cm^2.

For wavelength dependence experiments, another narrow bandpass filter with a bandwidth of 10 nm was additionally inserted. The intensity of the irradiation light became 0.57 mW/cm^2 at each wavelength. The absorption of MB was measured using a UV-vis spectrometer (Shimadzu UV 3600, D2 lamp for UV, Halogen lamp for Vis) with a slit width of 0.2 nm. An absorption spectrum was measured every minute. The UV irradiation was stopped during the spectral measurements. The photocatalytic reaction was monitored using the absorption spectrum of MB centered at 580 nm.

DDA calculations were performed with the DDSCAT program.[18] The calculated structures were either hemispherical or triangular. Al was assumed to be covered with Al oxide (Al_2O_3). At the contact region with air, the thicknesses of the Al_2O_3 layers were 6 nm for the 28 nm Al particles and 5 nm for the 34 and 80 nm particles.[10] The thickness of the Al_2O_3 layer at the contact region with the TiO_2 was fixed to 7 nm.[19] The spatial pitch was 1 nm. The dielectric functions of Al and Al_2O_3 in Ref. 20 were used. The polarization directions of incident light were both parallel to the sample plane and orthogonal to each other.

Figure 2 shows the observed photocatalytic reaction of TiO_2 with and without Al nanoparticles under the UV irradiation in the range 260–340 nm. The decay curves indicate the residual reaction rate of MB with respect to integrated irradiation time. The black line indicates the result without Al nanoparticles, whereas colored lines indicate the results with Al nanoparticles. The red, blue, and green colors indicate the rates obtained with Al nanoparticles having lateral sizes, D, of 28, 34, and 80 nm, respectively. For the 28 nm and 34 nm particles, the shape was approximated as a hemisphere, and for the 80 nm particles, the shape can be considered as a triangle. D is defined as the diameter of the hemisphere or the side length of the triangle. The height of the structure was the same as the evaporation thickness, that is, 30 nm. The net volume of the Al was actually smaller owing to surface oxidization. The estimated lateral sizes of the Al nanoparticles were 18 nm, 24 nm, and 70 nm.[14] Comparing the decay curves between samples with and without Al nanoparticles, the photocatalytic reaction rates of TiO_2 with Al nanoparticles were remarkably enhanced. These results demonstrate clearly the plasmonic enhancement of photocatalysis on TiO_2 by the UV-resonant Al nanoparticles.

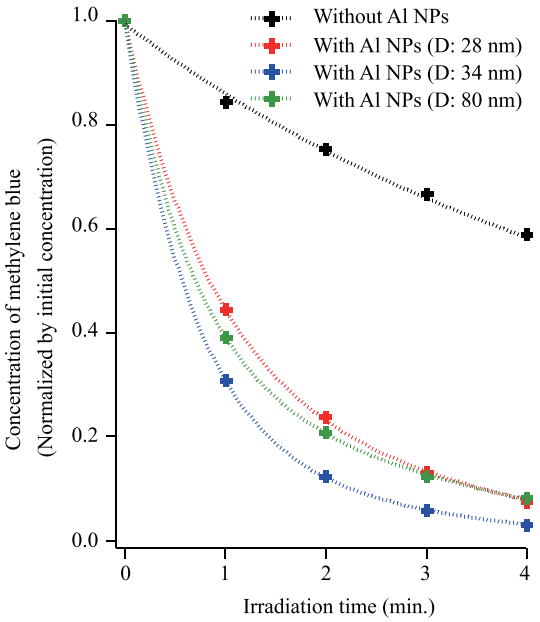

FIG. 2. Photocatalytic reaction with (colored) and without (black) Al nanoparticles under irradiation of UV light in the wavelength range of 260–340 nm. Red, blue, and green colors indicate the reaction obtained with Al nanoparticles having lateral sizes $D = 28$, 34, and 80 nm, respectively.

To evaluate the enhancement of the photocatalytic reaction rate, curve fitting was performed using the following equation:

$$f(t) = A + B\exp\left(-\frac{t}{\tau_1}\right) + C\exp\left(-\frac{t}{\tau_2}\right). \quad (1)$$

Here, $f(t)$ is a time-dependent function of the MB concentration during the photocatalytic reaction, A is the background signal, B and C indicate the area ratio inside and outside of the enhanced field, respectively, and τ_1 and τ_2 are the time constants of the MB decolorization rate with and without Al particles, respectively. The enhancement of the photocatalytic reaction rate is defined as τ_1/τ_2.

The values of τ_1/τ_2 with respect to lateral size D are summarized in Table I. Al nanoparticles with the size of 34 nm showed the larger enhancements than 28 nm and 80 nm Al nanoparticles. This is because the enhancement effect can be observed most dominantly at the absorption edge of TiO_2 (320 nm).[21] At shorter wavelengths, TiO_2 shows high quantum efficiency to initiate photocatalytic reactions, while at longer wavelengths, the efficiency is decreased and the higher photon density was required. As a result, 34 nm Al nanoparticles, which have the resonance peak at 320 nm, achieved to the highest enhancements.

TABLE I. Enhancement of photocatalytic reaction rate, τ_1/τ_2, under UV irradiation (range 260–320 nm) with nanoparticle sizes $D = 28$, 34, and 80 nm. See Eq. (1).

Size of A1 NPs, D (nm)	Enhancement of photocatalytic reaction rate (τ_1/τ_2)
28	9.8 ± 0.8
34	14.3 ± 0.9
80	12.9 ± 0.8

The 80 nm particles also show the larger enhancements as high as 12.9 than the 28 nm particles (exhibiting only 9.8). This can be because the 80 nm particles showed relatively high extinction efficiency at the band edge and also because they exhibit the high-integrated scattering efficiency at the wavelength region of 260 nm to 340 nm. Additionally, a triangular metallic nanoparticle in general supports the stronger electric field localized at the corner than a hemispherical metal nanoparticle. Therefore, the 80 nm triangular particle may have the advantage for plasmonic enhancement of photocatalytic reactions compared to the 28 nm hemisphere. In the case of photocatalysts other than TiO_2, the size of the plasmonic structure needs to be tuned. Furthermore, Table I also shows the dependence of the photocatalytic enhancement on nanoparticle size. We note that the enhanced field means the area where the field intensity drops to $1/e$ from the surface of the metal. In principle, as the diameter of the Al particles reduces, the $1/e$ distance becomes shorter, while the thickness of the oxide layer increases because of the curvature. The field enhanced area therefore decreases dramatically with decreasing particle size, which could explain the size dependence of the photocatalytic enhancement.

Finally, we investigated the dependence of the photocatalytic enhancement reaction on the irradiation wavelength. Figs. 3(a), 3(c), and 3(e) show the irradiation wavelength dependence of the photocatalytic enhancement for different values of D. Figs. 3(b), 3(d), and 3(f) show the calculated scattering efficiency corresponding to the structures in Figs. 3(a), 3(c), and 3(e), respectively. The wavelength axis in the simulation shows the converted wavelength which takes into account the effect of the TiO_2 substrate. The insets in Figs. 3(b), 3(d), and 3(f) show the field distributions at a wavelength of 320 nm, at half the height of the particles. In Figs. 3(b) and 3(d), distinct scattering peaks at 330 nm and 320 nm were observed for the 28 nm and 34 nm particles. For the 80 nm particles, peaks were not seen because the spectral width was broadened due to the large size of the Al particles. Moreover, judging from the field distributions (insets in Figs. 3(b) and 3(d)), plasmon resonances at 330 and 320 nm are assigned to the dipole mode, whereas the shorter one at 280 nm in Fig. 3(b) is assigned to the quadrupole mode. For each D, the wavelength dependence of the enhancement agreed with the calculated scattering efficiency. The higher photocatalytic enhancement at the scattering peaks is consistent with the existence of a stronger near-field confinement. Taking these conditions into account, the spectral similarity of the enhancement and the scattering efficiency suggests that the enhancement of the photocatalytic reaction originates

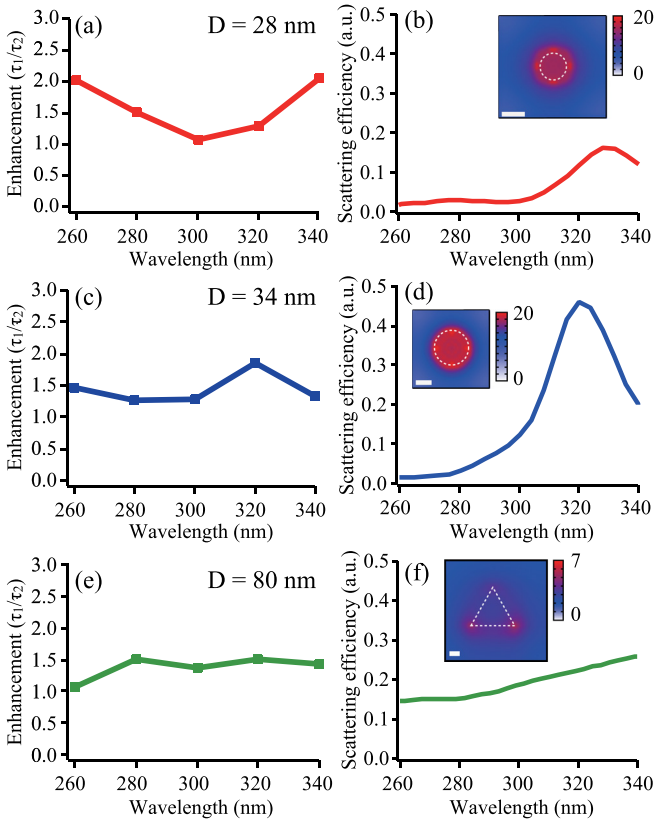

FIG. 3. Wavelength dependence of photocatalytic reaction enhancement. (a), (c), and (e) Experimental results with lateral sizes $D = 28$, 34, and 80 nm. (b), (d), and (f) Calculated scattering efficiency of Al nanoparticles corresponding to (a), (c), and (e), respectively. Insets show the cross-sectional view of the near-field distribution at a wavelength of 320 nm at the middle height of the particle. The color bar shows the field enhancement E_{NF}/E_0, where E_{NF} and E_0 indicate the field intensities of the near-field and the incident light, respectively. White dotted lines in the insets indicate the outlines of Al nanoparticles. The scale bars indicate 10 nm.

from the plasmonic properties of the Al nanoparticles. We estimated that an effect of "enhanced scattering" is smaller than the plasmonic effect because the particles are aligned in two dimensions and the density is low enough to avoid the effect of interactions between nanoparticles and multiple scattering between the structures. Other chemical effects on the photocatalytic reaction, for example, charge transfer and forced electron–hole pair separation, are considered to be absent in this system because the Al nanoparticles are surrounded by Al_2O_3 thick enough to avoid them.

In summary, the enhancement of photocatalytic activity in the deep-UV region was demonstrated using the plasmonic properties of Al nanostructures. A maximum increase to the photocatalytic reaction rate of about 14.3 times was obtained for particle sizes of 34 nm. Also the enhancement of the photocatalytic reaction rate was found to be dependent on plasmon resonance in the UV region, which was consistent with DDA simulation results. This study indicates the capability of utilizing UV plasmonic properties for the enhancement of photocatalyst performance where UV light is to be used. Plasmon-enhanced photocatalysis in the UV range is promising not only for conventional environmental applications but also it represents strategies for acquiring renewable and clean energy sources.

This work was financially supported by JSPS Grant-in-Aid for Scientific Research (S) No. 21226003. We thank Almar F. Palonpon for correcting the English in this manuscript. We also thank N. Takeyasu for helpful discussions.

[1]A. Fujishima and K. Honda, Nature **238**, 37 (1972).
[2]K. Hashimoto, H. Irie, and A. Fujishima, Jpn. J. Appl. Phys., Part 1 **44**, 8269 (2005).
[3]J. Lonnen, S. Kilvington, S. C. Kehoe, F. Al-Touati, and K. G. McGuigan, Water Res. **39**, 877 (2005).
[4]J.-M. Herrmann, Catal. Today **53**, 115 (1999).
[5]S. Hager and R. Bauer, Chemosphere **38**(7), 1549 (1999).
[6]A. Dhakshinamoorthy, S. Navalon, A. Corma, and H. Garcia, Energy Environ. Sci. **5**, 9217 (2012).
[7]S. Kawata, Appl. Spectrosc. **67**, 117 (2013).
[8]K. Awazu, M. Fujimaki, C. Rockstuhl, J. Tominaga, H. Murakami, Y. Ohki, N. Yoshida, and T. Watanabe, J. Am. Chem. Soc. **130**, 1676 (2008).
[9]X. M. Zhang, Y. L. Chen, R.-S. Liu, and D. P. Tsai, Rep. Prog. Phys. **76**, 046401 (2013).
[10]C. Langhammer, M. Schwind, B. Kasemo, and I. Zoric, Nano Lett. **8**(5), 1461 (2008).
[11]Y. Ekinci, H. H. Solak, and J. F. Löffler, J. Appl. Phys. **104**, 083107 (2008).
[12]G. H. Chan, J. Zhao, G. C. Schatz, and R. P. Van Duyne, J. Phys. Chem. C **112**, 13958 (2008).
[13]A. Taguchi, Y. Saito, K. Watanabe, S. Yijian, and S. Kawata, Appl. Phys. Lett. **101**, 081110 (2012).
[14]Y. Saito, M. Honda, K. Watanabe, A. Taguchi, Y. Song, and S. Kawata, J. Jpn. Inst. Met. **77**, 27 (2013).
[15]J. M. McMahon, G. C. Schatz, and S. K. Gray, Phys. Chem. Chem. Phys. **15**, 5415 (2013).
[16]H. W. Deckman and J. H. Dunsmuir, Appl. Phys. Lett. **41**, 377 (1982).
[17]J. C. Hulteen and R. P. Van Duyne, J. Vac. Sci. Technol., A **13**, 1553 (1995).
[18]B. T. Draine and P. J. Flatau, User Guide to the Discrete Dipole Approximation Code DDSCAT 7.2, 2012.
[19]S. Ikeno, T. Kawabata, H. Hayashi, K. Matsuda, S. Rengakuji, T. Suzuki, Y. Hatano, and K. Tanaka, Mater. Trans. **43**, 939 (2002).
[20]*Handbook of Optical Constants of Solids*, edited by E. D. Palik (Academic Press, New York, 1985), Vol. 1.
[21]N. Serpone, D. Lawless, and R. Khairutdinov, J. Phys. Chem. **99**, 16646 (1995).